

Tracing the Evolutionary History of Inositol, 1, 4, 5-Trisphosphate Receptor: Insights from Analyses of *Capsaspora owczarzaki* Ca²⁺ Release Channel Orthologs

Kamil J. Alzayady,¹ Arnau Sebé-Pedrós,^{*2} Rahul Chandrasekhar,¹ Liwei Wang,¹ Iñaki Ruiz-Trillo,^{2,3,4} and David I. Yule^{*1}

¹Department of Pharmacology and Physiology, University of Rochester

²Institut de Biologia Evolutiva, Universitat Pompeu Fabra-CSIC, Barcelona, Catalonia, Spain

³Departament de Genètica, Universitat de Barcelona, Barcelona, Catalonia, Spain

⁴Institució Catalana de Recerca i Estudis Avançats (ICREA), Barcelona, Catalonia, Spain

*Corresponding author: arnau.sebe@ibe.upf-csic.es; david_yule@urmc.rochester.edu.

Associate editor: Stuart Newfeld

Abstract

Cellular Ca²⁺ homeostasis is tightly regulated and is pivotal to life. Inositol 1,4,5-trisphosphate receptors (IP₃Rs) and ryanodine receptors (RyRs) are the major ion channels that regulate Ca²⁺ release from intracellular stores. Although these channels have been extensively investigated in multicellular organisms, an appreciation of their evolution and the biology of orthologs in unicellular organisms is largely lacking. Extensive phylogenetic analyses reveal that the IP₃R gene superfamily is ancient and diverged into two subfamilies, IP₃R-A and IP₃R-B/RyR, at the dawn of Opisthokonta. IP₃R-B/RyR further diversified into IP₃R-B and RyR at the stem of Filozoa. Subsequent evolution and speciation of Holozoa is associated with duplication of IP₃R-A and RyR genes, and loss of IP₃R-B in the vertebrate lineages. To gain insight into the properties of IP₃R important for the challenges of multicellularity, the IP₃R-A and IP₃R-B family orthologs were cloned from *Capsaspora owczarzaki*, a close unicellular relative to Metazoa (designated as CO.IP₃R-A and CO.IP₃R-B). Both proteins were targeted to the endoplasmic reticulum. However, CO.IP₃R-A, but strikingly not CO.IP₃R-B, bound IP₃, exhibited robust Ca²⁺ release activity and associated with mammalian IP₃Rs. These data indicate strongly that CO.IP₃R-A as an exemplar of ancestral IP₃R-A orthologs forms bona fide IP₃-gated channels. Notably, however, CO.IP₃R-A appears not to be regulated by Ca²⁺, ATP or Protein kinase A-phosphorylation. Collectively, our findings explore the origin, conservation, and diversification of IP₃R gene families and provide insight into the functionality of ancestral IP₃Rs and the added specialization of these proteins in Metazoa.

Key words: calcium release channels, inositol 1, 4, 5-trisphosphate receptor, *Capsaspora owczarzaki*.

Introduction

Since the origin of life in the primordial ocean, calcium ions (Ca²⁺) have played pivotal roles in the survival, proliferation and growth of all life forms (Case, et al. 2007; Plattner and Verkhratsky 2013; Verkhratsky and Parpura 2014). Both prokaryotes and eukaryotes have evolved complex molecular systems of buffers, channels, transporters, pumps, and exchangers to ensure Ca²⁺ homeostasis and enable the regulation of downstream effectors (Berridge, et al. 2000; Berridge, et al. 2003; Verkhratsky and Parpura 2014). The appropriate spatiotemporal activation of Ca²⁺ sensitive effectors, in turn, is utilized to coordinate a myriad of cellular activities (Berridge, et al. 2003; Iino 2010). To control Ca²⁺ influx and extrusion, the plasma membrane in eukaryotes is studded with Ca²⁺ permeable channels including voltage-gated and ligand-gated Ca²⁺ channels, plasma membrane Ca²⁺ ATPase, store-operated Ca²⁺ channels, and transient receptor potential (TRP) channels (Catterall 2000; Clapham 2007; Gees, et al. 2010; Brini, et al. 2012). Furthermore, the acquisition of intracellular membranes and evolution of organelles have enabled

eukaryotes to sequester Ca²⁺ and establish intracellular stores that can be emptied and refilled as needed (Berridge, et al. 2000; Case, et al. 2007; Plattner and Verkhratsky 2013; Verkhratsky and Parpura 2014). These Ca²⁺ stores are equipped with pumps which replenish the stores and thus maintain low intracellular [Ca²⁺], and channels which when gated, direct the flow of Ca²⁺ into the cytoplasm. The inositol 1,4,5-trisphosphate receptors (IP₃Rs) and ryanodine receptors (RyRs) are the main protein families that regulate Ca²⁺ release from intracellular stores (Fill and Copello 2002; Foskett, et al. 2007). In mammals, IP₃Rs are encoded by three different genes (*ITPR1*, *ITPR2*, and the *ITPR3*) and the proteins are expressed in a distinct but overlapping manner in various tissues. IP₃Rs form homo- and heterotetrameric channels, which are predominantly localized in membranes of the endoplasmic reticulum (ER) (Bezprozvanny 2005; Foskett, et al. 2007). The RyR family also consists of three distinct genes (*RyR1*, *RyR2*, and *RyR3*) that similarly assemble to form tetrameric channels and mediate Ca²⁺ release from sarcoplasmic reticulum and ER (Fill and Copello 2002). RyR1 is enriched in

skeletal muscle, whereas RyR2 is primarily expressed in cardiac muscle. RyR3 is widely expressed in various tissues but enriched particularly in the brain (Giannini, et al. 1995). Although IP₃R and RyR are structurally related, they are modulated differently (Fill and Copello 2002; Foskett, et al. 2007). IP₃Rs are activated by IP₃ produced in response to the stimulation of cell surface receptors (Berridge, et al. 2000; Foskett, et al. 2007). RyR channels are stimulated primarily by Ca²⁺, whereby small elevations of Ca²⁺ in the vicinity of the RyR channels trigger channel activation and amplification of Ca²⁺ signals (Fill and Copello 2002). IP₃R and RyR-mediated Ca²⁺ release is essential to mammalian life (Futatsugi, et al. 2005) and is involved in regulating a plethora of cellular activities including metabolism, cell cycle, muscle contraction, fertilization, endocytosis, exocytosis, phagocytosis, and apoptosis (Berridge, et al. 2000; Fill and Copello 2002). Mutations of members of IP₃R and RyR families have been associated with many debilitating human diseases (Betzenhauser and Marks 2010; Bezprozvanny 2011).

Although the molecular components of Ca²⁺ handling apparatus have been extensively investigated in many multicellular eukaryotes, very scarce information is available on their counterparts in unicellular organisms (Bezprozvanny 2005; Zhang, et al. 2007). However, several recent bioinformatics and phylogenetic studies that surveyed the sequenced genomes of a diverse array of unicellular eukaryotic species have revealed a rich repertoire of genes encoding proteins predicted to be involved in Ca²⁺ signaling and which had previously been widely presumed to be unique to higher animals (Cai 2008; Cai and Clapham 2008, 2012; Cai, et al. 2014). Although these studies have highlighted sequence conservation of a number of components of the unicellular Ca²⁺ machinery, functional verification of the annotated genes is still lacking. Indeed, dissecting the function of molecules from the presumed unicellular ancestors has potential to provide meaningful insights into how diverse organisms adapt and respond to their environment (King 2004). In addition, given the universality of Ca²⁺ signaling, studying the conservation and innovations of the Ca²⁺ signaling machinery can shed new light on the emergence and evolution of multicellular organisms from unicellular ancestors. Specifically, whether the transition from unicellularity to a multicellular existence is accompanied by more sophisticated Ca²⁺ systems or novel regulatory modes is not known. More importantly, understanding how these pathways have functioned and shaped early life forms will help better address many outstanding pathophysiological questions.

Here, we have traced the evolutionary history of IP₃R and RyR by searching the complete genomes or transcriptome sequences of 102 taxa representing all eukaryotic supergroups. To our knowledge, this represents the most comprehensive phylogenetic analyses of IP₃R and RyR performed to date. Furthermore, we have cloned and characterized two IP₃R orthologs, designated CO.IP₃R-A and CO.IP₃R-B (belonging to the IP₃R-A and IP₃R-B subfamilies) from the filasterean *Capsaspora owczarzewski*, a close relative to Metazoa (Ruiz-Trillo, et al. 2004; Steenkamp, et al. 2006; Ruiz-Trillo, et al. 2008; Torruella, et al. 2012). We demonstrate that

CO.IP₃R-A, but not prominently CO.IP₃R-B, is an authentic IP₃-gated Ca²⁺ release channel. However, in contrast to metazoan IP₃Rs, we show that CO.IP₃R-A activity is not prominently modulated by the key regulators: ATP, Ca²⁺, or Protein kinase A (PKA) phosphorylation. These data imply that the acquisition of these modes of regulation might be a specialization of metazoans. In total, our findings provide a comprehensive view of the evolution of IP₃R and RyR channels and offer the first glimpse to the functionality of IP₃Rs that are believed to be the relatives of animal IP₃Rs, which diverged in antiquity.

Results

Evolutionary History of IP₃Rs and RyRs

We studied the evolutionary history of IP₃R/RyR proteins in eukaryotes. In particular, we searched the complete genomes or transcriptomes of 102 taxa representing all eukaryotic supergroups (supplementary table S1, Supplementary Material online). Our phylogenetic analyses (supplementary figs. S1 and S2, Supplementary Material online) indicate that IP₃Rs are an ancient eukaryotic gene family, which was secondarily lost several times independently within eukaryotes, especially in Bikont lineages (including Rhizaria, Glaucophyta, Embryophyta, and Rhodophyta). The family diverged into two paralog subfamilies (IP₃R-A and IP₃R-B/RyR) at the stem of Opisthokonts (fig. 1). The family further diversified at the stem of Filozoa, which includes Metazoa, Choanoflagellata, and Filasterea. Thus, IP₃R-B/RyR gave rise to IP₃R-B and RyR, the latter with a unique protein domain architecture that largely differs from the canonical IP₃R domain architecture (fig. 1). Our analysis shows that the ancestral IP₃R has a unique domain structure, shared by most extant eukaryotic IP₃Rs, including the IP₃R-A and IP₃R-B/RyR subfamilies, and is composed of a recognizable N-terminal IP₃-binding domain, a MIR domain, two RYDR-ITPR domains, a RIH-associated domain, and a C-terminal ion transport domain. One particular Bikont group, the ciliates (represented here by *Paramecium tetraurelia* and *Tetrahymena thermophila*), exhibits a massive expansion of IP₃Rs, with tens of homologs that broadly cluster in the phylogeny into two different groups (supplementary fig. S1, Supplementary Material online). The independent losses observed in several eukaryotic lineages (with the current taxon sampling) and the great expansion of ciliates highlight the plasticity of this family. Interestingly, all IP₃R subfamilies were secondarily lost in almost all fungi. Indeed, we could only identify a putative IP₃R-B/RyR in two zygomycetes, but both IP₃R-A and IP₃R-B/RyR are clearly present in Nucleariids, the sister group to Fungi (supplementary fig. S2, Supplementary Material online). Our findings support the premise that the three families are present in almost all filasterean, choanoflagellate, and metazoan species examined, except for the ctenophore *Mnemiopsis leyidi* that has lost both RyR and IP₃R-B, and *Homo sapiens* that has lost IP₃R-B (as have all vertebrates).

We next analyzed the conservation of functional amino acid motifs in these three gene families (supplementary table S2, Supplementary Material online). We found that most of

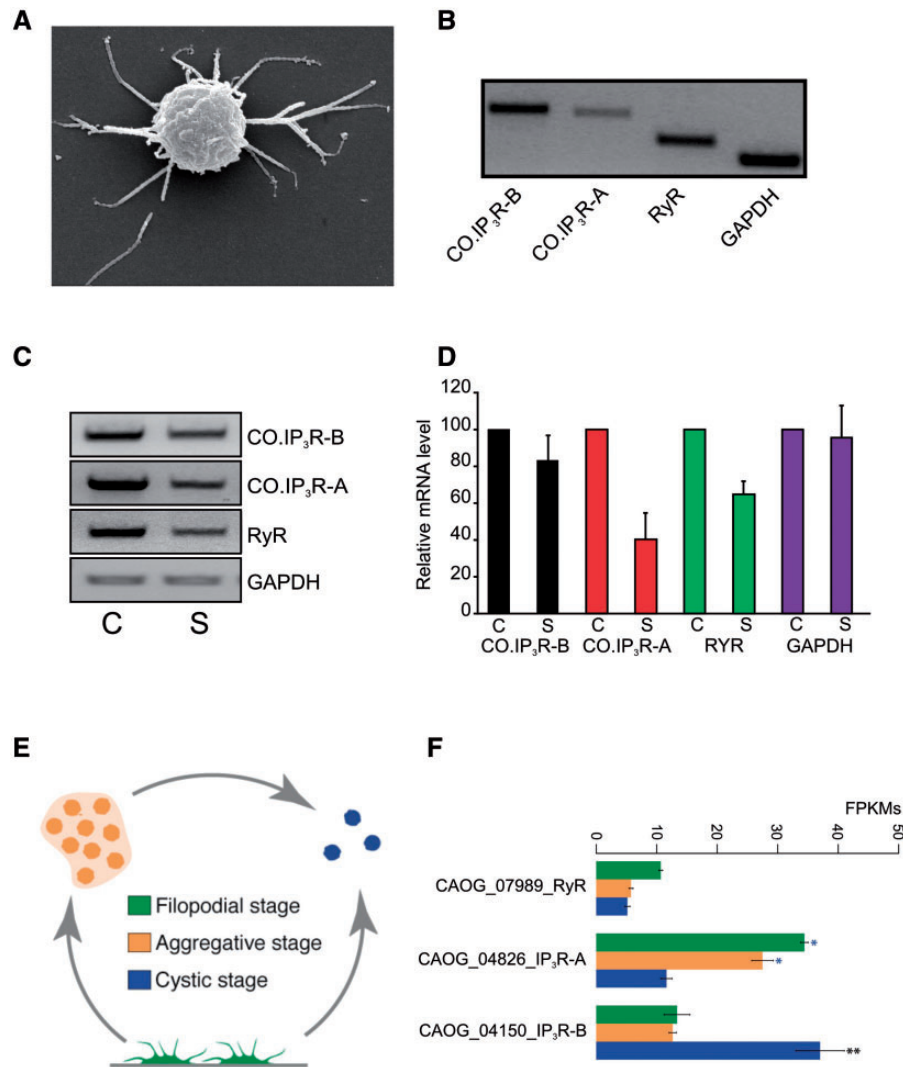


Fig. 2. Expression and modulation of *Capsaspora owczarzaki* COIP₃R-A, COIP₃R-B, and RyR. (A) Scanning electron microscopy micrograph of *C. owczarzaki* filopodial stage amoeba. (B) Expression of COIP₃R-A, COIP₃R-B, RyR, and GAPDH genes in *C. owczarzaki* determined by RT-PCR. (C) Representative semiquantitative RT-PCR of COIP₃R-A, COIP₃R-B, and RyR in *C. owczarzaki* growing under control (C) or starvation (S) conditions. GAPDH served as a loading control. (D) Histograms generated from densitometric quantification of DNA gels as shown in (C). Values were normalized to the controls. Data represent mean \pm SD of ≥ 3 independent experiments. (E) A schematic diagram depicting the three stages of *C. owczarzaki* life cycle: Aggregative, filopodial, and cystic stages. (F) Expression of COIP₃R-A, COIP₃R-B, and RyR genes in different life stages of *C. owczarzaki*. Barplots indicate the FPKM values of each gene in the different stages color-coded as in (E). Asterisks indicate that the gene is significantly differentially expressed in both (two asterisks) or only one (one asterisk) pairwise comparison (aggregative vs. filopodial and aggregative vs. cystic). Bars show standard error.

unicellular eukaryotes have been instrumental in illuminating the genetic and biochemical innovations that have contributed to the rise and diversity of multicellular animals (King, et al. 2008; Sebe-Pedros, et al. 2011; Fairclough, et al. 2013; Suga, et al. 2013). The genome of *C. owczarzaki* encodes several components of the Ca²⁺ signaling machinery (Cai and Clapham 2012). These include two IP₃R-like genes (designated as COIP₃R-A and COIP₃R-B), a single ryanodine receptor (RyR), a two-pore channel, TPR channels, Na⁺/K⁺ exchanger, and Orai. To gain insight into the biology of premetazoan Ca²⁺ machinery, we focused on COIP₃R and RyR channels in *C. owczarzaki*. We initially assessed the expression of these genes using reverse transcription polymerase chain reaction (RT-PCR) with a set of gene-specific primers and total RNA isolated from *C. owczarzaki* cells harvested in log-growth

phase. Figure 2B shows that under these conditions, *C. owczarzaki* expressed COIP₃R-A, COIP₃R-B, and RyR in addition to the house-keeping gene glyceraldehyde 3-phosphate dehydrogenase (GAPDH).

Differential Expression of CO-IP₃R-A, CO-IP₃R-B, and RyR

IP₃Rs expression levels and activity have been shown to undergo significant regulation during various developmental and metabolic conditions in numerous organisms and in different cell types (Taylor, et al. 1999; Hashimoto, et al. 2013). Furthermore, although *C. owczarzaki* is thought to adopt a symbiotic existence, it is not clear whether it ventures into freshwater and lives as free-living amoeba where it might encounter nutrient fluctuations (Stibbs, et al. 1979; Owczarzak, et al. 1980; Hertel, et al. 2002). To investigate

whether the expression of CO-IP₃R-A, CO-IP₃R-B or RyR is regulated in response to environmental cues, *C. owczarzaki* cells were grown in either complete culture medium or water for 24 h. Previous studies have indicated that *C. owczarzaki* can survive in spring water up to 5 days (Stibbs, et al. 1979). Total RNA was isolated and semiquantitative RT-PCR was performed to determine the relative transcriptional levels of Co.IP₃R-A, CO.IP₃R-B, and RyR. Figure 2C and D shows that the expression levels of Co.IP₃R-A, and RyR but not CO.IP₃R-B were significantly downregulated by nutrient deprivation. The level of GAPDH did not change upon treatment. These data indicate that the expression of these genes is regulated differently in response to environmental cues and thus suggest that there might be a link between the function of these genes and metabolic adaptation. Moreover, we have shown previously that *C. owczarzaki* has three stages in its life cycle (fig. 2E) (Sebe-Pedros, et al. 2013). The filopodial stage represents a freely motile amoeba exhibiting long filopodia extending in every direction from the cell body. *Capsaspora owczarzaki* enters the cystic stage when it withdraws its filopodia and forms smaller round-shaped double-walled cysts (Stibbs, et al. 1979; Sebe-Pedros, et al. 2013). In the aggregative stage, population of cells becomes enmeshed in extracellular matrix. The transition from one stage to the other is associated with significant transcriptional modulation. Specifically, it has been shown that the aggregative stage is associated with upregulation of genes implicated in metazoan multicellularity (Sebe-Pedros, et al. 2013). To examine the expression levels of CO.IP₃R-A, CO. IP₃R-B, and RyR in the three life stages of *C. owczarzaki*, total RNA was isolated and RNA sequencing libraries were constructed and sequenced using next generation sequencing. Figure 2F shows that RyR is upregulated in the filopodial stage. *C. owczarzaki* IP₃Rs are reciprocally expressed: CO.IP₃R-A is upregulated in the filopodial and aggregative stages, whereas CO.IP₃R-B is upregulated in the cystic stage only. Although this study does not address the specific functions of CO.IP₃R-A and CO.IP₃R-B in *C. owczarzaki*, this clear distinct expression pattern of the individual proteins suggests a subspecialization of function of these two subfamilies of IP₃R in *C. owczarzaki*.

Generation of Stable Cell Lines Expressing CO.IP₃R-A and CO.IP₃R-B

As exemplars of the behavior of an important component of the *C. owczarzaki* Ca²⁺ signaling machinery, we cloned the coding sequences of CO.IP₃R-A and CO.IP₃R-B. CO.IP₃R-A is 9,699 bp encoding a 3,232-amino acid protein with an apparent molecular weight of 352 kDa, whereas CO.IP₃R-B is 7,962 bp and encodes a 2,653-amino acid protein with an estimated molecular weight of 298 kDa. Both constructs were fused with an HA tag and expressed in DT40-3KO, chicken B-lymphoma cell lines that are devoid of any endogenous IP₃Rs (Sugawara, et al. 1997). Figure 3A shows an immunoblot analysis of cell lysates prepared from DT40-3KO expressing the indicated constructs. HA-reactive bands of appropriate molecular mobility were detected in CO.IP₃R-A and

CO.IP₃R-B, and as expected no HA immunoreactivity was detected in the DT40-3KO.

CO.IP₃R-A, but not CO.IP₃R-B, is an IP₃-Gated Ca²⁺ Release Channel

IP₃ Binds Only to CO.IP₃R-A

The structure of mammalian IP₃R1 can be divided into three functional domains: The N-terminal ligand-binding domain (amino acids 1-604), the central regulatory domain (amino acids 605-2275), and the C-terminal channel domain (amino acids 2276-2749) containing six membrane spanning regions and the cytosolic tail (Bezprozvanny 2005). Multiple sequence alignment of the deduced amino acid sequences of CO.IP₃R-A revealed 15.5% amino acid identity and 27% amino acid similarity with CO.IP₃R-B. However, rIP₃R1 shares 37.4% identity and 47.6% similarity with CO.IP₃R-A, and 18.3% identity and 31.8% amino acid similarity with CO.IP₃R-B. In addition, comparing the ligand-binding domain of rIP₃R1 reveals a 61.6% identity and 73.5% similarity with that of CO.IP₃R-A, and 20.6% identity and 34.9% similarity with that of CO.IP₃R-B. The relative differences in the degree of conservation between mammalian IP₃R, representative of IP₃R-A paralogs, and CO.IP₃R-A and CO.IP₃R-B are again suggestive of distinct subspecialization of IP₃R-B family members.

Furthermore, there are ten basic residues in the ligand-binding core that are proposed to form a binding pocket to accommodate the negatively charged IP₃ molecule (Yoshikawa, et al. 1996). All ten residues, constituting the IP₃-binding pocket are conserved in CO.IP₃R-A; however, only seven are present in CO.IP₃R-B (supplementary fig. S3A and table S2, Supplementary Material online). In light of the overall amino acid conservation and in particular the similarity of the ligand-binding domain, we sought to determine whether the *C. owczarzaki* IP₃R proteins bind IP₃. HA-tagged CO.IP₃R-A and CO.IP₃R-B were immunopurified and specific binding capacity was determined as detailed in Materials and Methods. Figure 3A shows that CO.IP₃R-A specifically bound radioactive IP₃. In contrast, radioactivity associated with CO.IP₃R-B was comparable to beads alone. These data indicate that CO.IP₃R-A, but not CO.IP₃R-B, indeed binds the natural ligand of IP₃Rs. To better appreciate the binding potency of CO.IP₃R-A, the protein was immunopurified and incubated with increasing concentrations of cold IP₃. Figure 3B shows a competitive IP₃-binding assay and indicates that CO.IP₃R-A exhibits an EC₅₀ of 68 ± 25 nM, comparable to that of mammalian IP₃R1 (Cui, et al. 2004). In total, the ability of CO.IP₃R-A to bind [³H]IP₃ is entirely consistent with the precise conservation of structural determinants required for IP₃ binding between CO.IP₃R-A and mammalian IP₃Rs. These findings also indicate that the absence of positively charged residues corresponding to K249, R265, and R269 in rIP₃R1 is sufficient to render the CO.IP₃R-B IP₃ insensitive (Yoshikawa, et al. 1996). Given the lack of absolute conservation of the IP₃-binding pocket in any IP₃R-B family member, it is tempting to speculate that IP₃R-B family members may not be activated by IP₃ and are specialized for distinct, as yet undetermined functions.

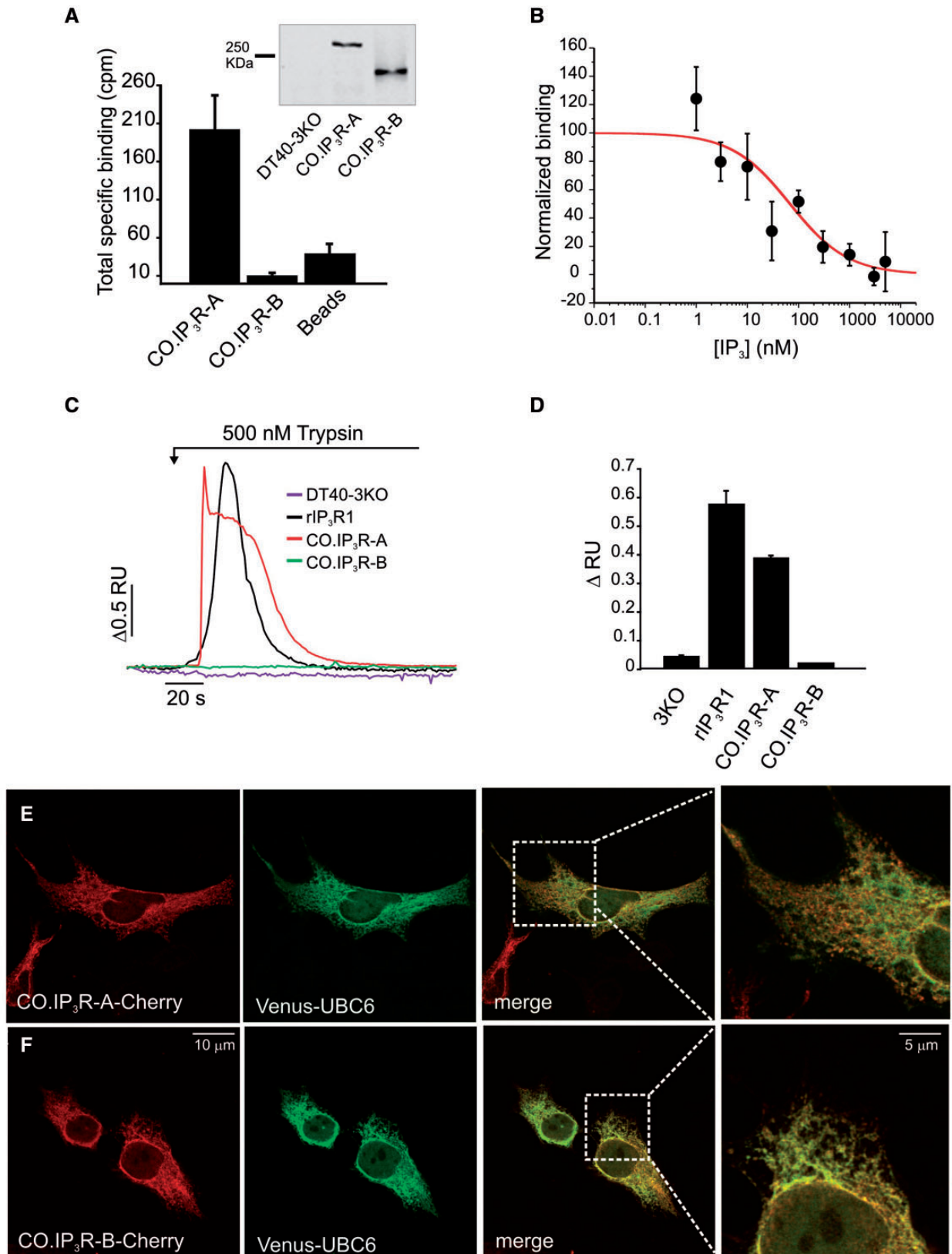


Fig. 3. Generation of stable cells and assessing ligand binding, functionality and subcellular localization of CO.IP₃R-A and CO.IP₃R-B. (A) Blot: Lysates prepared from DT40-3KO or DT40-3KO cells stably expressing HA-tagged CO.IP₃R-A or CO.IP₃R-B were fractionated on 5% SDS-PAGE and processed in immunoblots with HA11 antibodies. Representative experiment is shown. Histograms: HA-tagged CO.IP₃R-A and CO.IP₃R-B were immunopurified and incubated with tritiated IP₃ without or with cold IP₃. Bound radioactivity as CPM was measured by scintillation. Protein A/G agarose beads were used as negative control. Total specific binding was determined by subtracting CPM in the presence of cold IP₃ from CPM in its absence. (B) HA-tagged CO.IP₃R-A was immunopurified and incubated with tritiated IP₃ and increasing concentrations of cold IP₃. Specific binding is determined by subtracting CPM values obtained in the presence of 50 μM cold from the CPM values obtained with other conditions. Normalized specific binding from three to

(continued)

IP₃-Induced Ca²⁺ Release Only by CO.IP₃R-A

The sequence comparison between the C-terminal regions of CO.IP₃R-A and CO.IP₃R-B and mammalian IP₃Rs shows a significant conservation of certain motifs essential for mammalian IP₃R activity (supplementary fig. S3B, Supplementary Material online). Even though hydropathy analyses revealed more hydrophathic stretches toward the C-terminus of both CO.IP₃R-A and CO.IP₃R-B consistent with the known IP₃R structure, their topological structures could not reliably be determined using in silico approaches. Therefore, the location and number of transmembrane (TM) helices will await future experimental studies. Notably, amino acid sequences corresponding to the fifth TM domain, pore helix, and the pore lining helix are very conserved (supplementary fig. S3B, Supplementary Material online). Interestingly, sequence alignment reveals the presence of the characteristic selectivity filter in the putative channel pore in CO.IP₃R-A but not CO.IP₃R-B. However, CO.IP₃R-A contains the motif GGIGD instead of the

signature sequence GGVGD typical of mammalian IP₃Rs (supplementary table S2, Supplementary Material online, but see above). As such, the relatively high degree of amino acid identity and structural homology between CO.IP₃R-A and CO.IP₃R-B and mammalian IP₃R suggest that these *C. owczarzewski* proteins might have the necessary molecular constituents to assemble and behave as genuine IP₃-gated Ca²⁺ release channels.

We therefore next investigated whether CO.IP₃R-A or CO.IP₃R-B is capable of forming functional IP₃-gated Ca²⁺ release channels. The intracellular [Ca²⁺]_i was measured in DT40-3KO cells stably expressing HA-tagged CO.IP₃R-A or HA-tagged CO.IP₃R-B as detailed in Materials and Methods. Cells were stimulated with 500 nM trypsin to activate the G-protein coupled, protease-activated receptor (PAR) and induce IP₃ formation. The resting [Ca²⁺]_i was not significantly different in DT40-3KO or in DT40-3KO expressing CO.IP₃R-A, CO.IP₃R-B or rIP₃R1 suggesting that *C. owczarzewski* proteins do

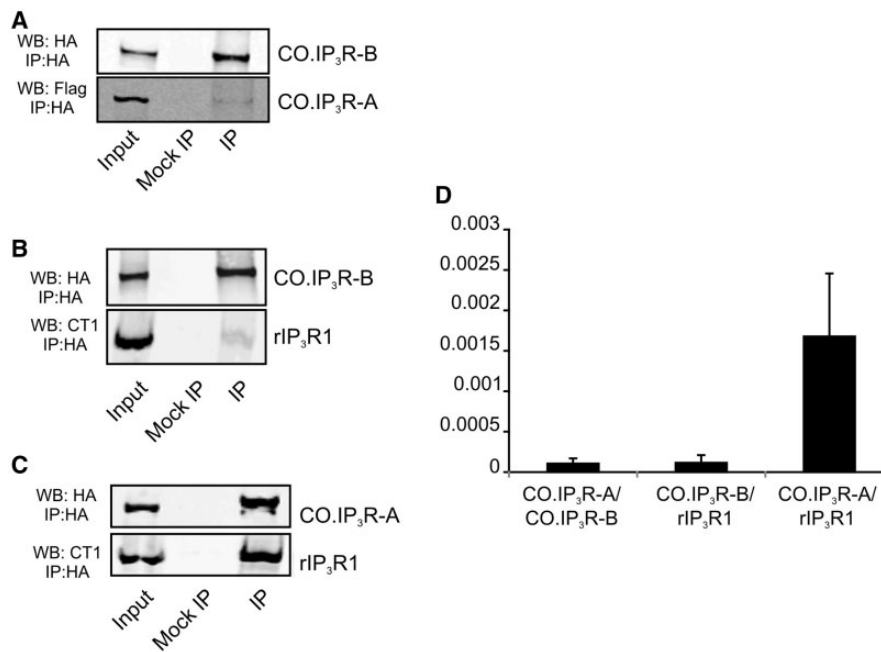


Fig. 4. Oligomerization of CO.IP₃R-A and CO.IP₃R-B. HEK293T was transfected with flag-tagged CO.IP₃R-A and HA-tagged CO.IP₃R-B (A), HA-tagged CO.IP₃R-B and rIP₃R1 (B) or HA-tagged CO.IP₃R-A and rIP₃R1 (C). Lysates were prepared from transfected cells and immunoprecipitated with the indicated antibodies. Mock-immunoprecipitates were carried out identically but with the omission of the immunoprecipitating antibody. The input and immunoprecipitates were processed in immunoblots and visualized by LI-COR Odyssey infrared imaging system. Representative experiments are shown. (D) Histograms depicting quantification of coimmunoprecipitated proteins shown in (A)–(C). The relative immunoreactivities of proteins were quantified and expressed as the ratios of coimmunoprecipitated proteins normalized to the amounts of the coimmunoprecipitated proteins in the input and divided by the immunoprecipitated proteins. Data are presented as mean ± SD of ≥3 independent experiments.

Fig. 3. Continued

four experiments were averaged and used for nonlinear curve fitting. (C) DT40-3KO or DT40-3KO stably expressing various IP₃R constructs were loaded with Fura-2AM, and stimulated with 500 nM trypsin to induce IP₃ formation. Ca²⁺ release was measured as a change in the 340/380 fluorescence ratios. Ratio values were normalized to the initial baseline. Shown are representative Ca²⁺ traces from the indicated cell lines. (D) Bar graphs depict the average maximum change over basal 340/380 fluorescence ratios resulting from trypsin stimulation of cells expressing the indicated constructs. Experiments were repeated at least three times with greater than 40 cells analyzed in each experiment. Data are presented as mean ± SE. HEK293 cells coexpressing Venus-UBC6 along with CO.IP₃R-A-mCherry (E) or CO.IP₃R-B-mCherry (F) were grown on glass coverslips, fixed with methanol, mounted on a slide. Images were captured using two-photon confocal microscopy.

not disrupt ER integrity or form leaky channels (data not shown). As shown previously, DT40-3KO cells do not respond to PAR activation being devoid of any IP₃R. In contrast, stimulation of rIP₃R1 expressing cells elicited a marked increase in [Ca²⁺]_i (fig. 3C and D). Remarkably, cells expressing CO.IP₃R-A responded robustly to PAR activation. However, cells expressing CO.IP₃R-B were not responsive, even to higher concentrations of trypsin (fig. 3C and D, and data not shown). Interestingly, cells expressing CO.IP₃R-A produced a very characteristic spear-shaped transient that fell to a plateau before decaying. Experiments performed in the absence of extracellular Ca²⁺ indicate that CO.IP₃R-A mediated Ca²⁺ release from internal stores (data not shown). Additional experiments show that HA-tagged, Flag-tagged as well as mCherry-tagged CO.IP₃R-A mediate Ca²⁺ release, which is not significantly different from nontagged CO.IP₃R-A suggesting that these tags do not interfere with channel function (data not shown). In total, these findings strongly demonstrate that CO.IP₃R-A binds IP₃ and forms bona fide IP₃R-sensitive Ca²⁺ channels like the related mammalian IP₃R-As, whereas CO.IP₃R-B does not bind IP₃ and thus does not form IP₃R-sensitive Ca²⁺ channels under these experimental conditions. Whether CO.IP₃R-A and B function as IP₃-sensitive Ca²⁺ release channels in *C. owczarzaki* remains formally to be established.

Subcellular Localization CO.IP₃R-A and CO.IP₃R-B in Mammalian Cells

Mammalian IP₃Rs are predominantly ER-resident proteins. However, studies have shown that IP₃R may also be targeted to the Golgi apparatus, secretory vesicles, and plasma membrane (Vermassen, et al. 2004). In addition, recent functional and immunostaining studies have shown that IP₃R in *Trypanosoma brucei* is localized to acidocalcisomes and IP₃R-like proteins have been shown to reside in the various subcompartments of the osmoregulatory system of *P. tetraurelia* (Ladenburger, et al. 2009; Huang, et al. 2013). To analyze the subcellular distribution of CO.IP₃R-A and CO.IP₃R-B, fusion proteins containing mCherry at the C-terminus of CO.IP₃R-A and CO.IP₃R-B were transiently expressed in HEK293 cells. A vector encoding mCherry protein alone was used as a control. [Supplementary figure S4, Supplementary Material](#) online, shows that although the mCherry protein is homogeneously distributed in both nucleus and the cytoplasm, the distribution of the fusion proteins containing CO.IP₃R-A and CO.IP₃R-B was predominantly perinuclear and reticular suggesting that they were targeted to the ER. To confirm this ER localization, CO.IP₃R-A and CO.IP₃R-B mCherry fusion proteins were transiently expressed in HEK293 cells along with a Venus fluorescent protein fused to the C-terminal ER localization sequence of UBC6 (Varnai, et al. 2005). [Figure 3E and F](#) clearly shows colocalization of Venus-UBC6 with CO.IP₃R-A and CO.IP₃R-B suggesting that the latter two constructs are targeted to the ER membranes like their mammalian counterparts. Indeed, a quantitative assessment of colocalization of the two fluorophores using Pearson correlation coefficient yielded values

greater than 0.93 (1.0 equates to a perfect positive correlation) for Venus-UBC6 and either CO.IP₃R-A or CO.IP₃R-B, indicating strong correlation for the localization of each fluorophore-tagged protein. Consistent with this localization, electron microscope studies have revealed that *C. owczarzaki* contains typical eukaryotic intracellular organelles such as rough and smooth ER, Golgi apparatus, phagosomes, lipid vacuoles, glycogen droplets, and mitochondria (Stibbs, et al. 1979). Therefore, whether CO.IP₃R-A and CO.IP₃R-B might also be targeted to non-ER membranes will require further experiments to immunolocalize these proteins in *C. owczarzaki* cells.

Oligomerization of CO.IP₃R-A and CO.IP₃R-B with Mammalian IP₃Rs

Mammalian IP₃R subtypes form homo- and heterotetrameric channels, which have been proposed to fine-tune and provide added regulatory diversity to intracellular Ca²⁺ signals (Bezprozvanny 2005; Foskett, et al. 2007). It has been proposed that the primary oligomerization determinants are located in the TM domains TM5 and TM6 and secondary oligomerization signals are located in TM1–4 (Joseph, et al. 1997). To determine whether CO.IP₃R-A and CO.IP₃R-B physically associate with each other or with mammalian IP₃Rs, coimmunoprecipitation experiments were performed. Total HEK293 cell lysates containing flag-tagged CO.IP₃R-A and HA-tagged CO.IP₃R-B were mock-immunoprecipitated with protein A/G beads or immunoprecipitated with HA.11 antibodies. [Figure 4A and D](#) demonstrates that CO.IP₃R-A and CO.IP₃R-B only weakly interact in this cellular context. In addition, HA-tagged CO.IP₃R-B did not associate with rIP₃R1 ([fig. 4B and D](#)). In contrast, when coexpressed in HEK293 cells, HA-tagged CO.IP₃R-A readily associated with rIP₃R1 ([fig. 4C and D](#)) and rIP₃R3 ([supplementary fig. S5, Supplementary Material](#) online). These findings suggest that, contrary to mammals, where heterotetramerization of IP₃R-A paralogs occurs, CO.IP₃R-A and CO.IP₃R-B are unlikely to form heteromeric channels. These data emphasize the divergence in structure of the IP₃R-A and IP₃R-B families and are consistent with the independent expression patterns observed during the *C. owczarzaki* life cycle. Establishing whether CO.IP₃R-A and CO.IP₃R-B interact in vivo will await the development of specific antibodies. Overall, our results indicate that profound differences between the IP₃R-A and IP₃R-B (not present in mammals) subfamilies are likely to exist. Notably, however, these data clearly demonstrate that COIP₃R-A has conserved oligomerization interfaces compatible with allowing the formation of heteromeric structures with IP₃R-A family members (represented by rIP₃R1 and rIP₃R3) from distantly related mammals.

Regulation of CO.IP₃R-A Activity

The central and largest region of IP₃R molecule is called the regulatory domain and it is the least conserved module among mammalian IP₃R isoforms (Bezprozvanny 2005; Foskett, et al. 2007). This region couples ligand binding in the N-terminus to the channel pore located at the extreme

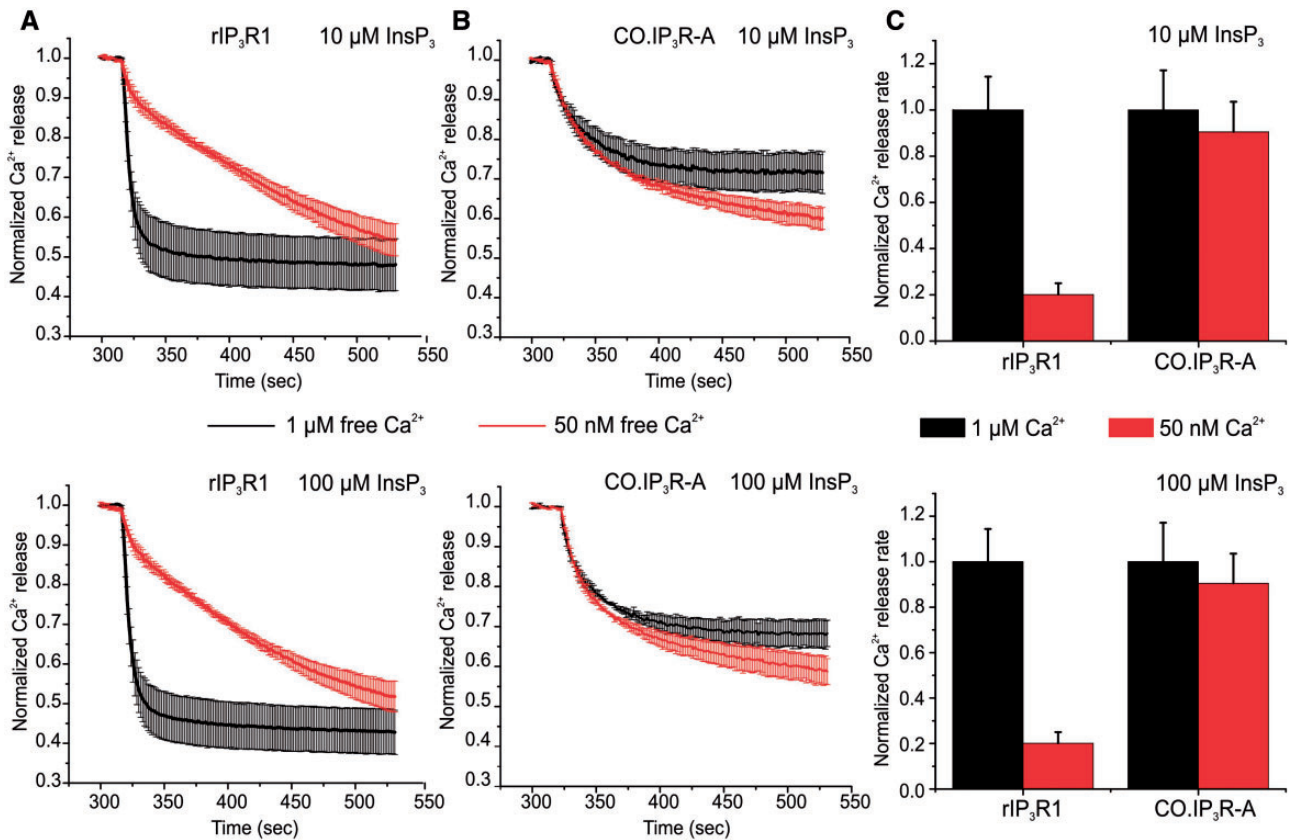


Fig. 5. Modulation of CO.IP₃R-A by Ca²⁺. DT40.3KO cells expressing rIP₃R1 (A) or CO.IP₃R-A (B) were loaded with Mag-Fluo4 and permeabilized. 1.5 mM ATP was added to activate SERCA pumps and fill intracellular calcium stores. Cells were then stimulated with the indicated concentrations of IP₃ in the absence (black traces) or presence of BAPTA (red traces). Fluorescence was normalized to the initial fluorescence intensity prior to release by IP₃. (C) Histograms depict maximum calcium release normalized and expressed as a percentage of control from experiments in (A) and (B).

C-terminus. It also serves as the binding sites for many important regulatory factors, such as ATP, Ca²⁺, phosphorylation, calmodulin, caspase, and phosphatases. The exact boundaries of the regulatory domain in *C. owczarzaki* proteins are not readily identifiable. In the following sections, we investigate whether a conserved structural and functional capability is present in CO.IP₃R-A to participate in three modes of regulation, which are highly important for shaping Ca²⁺ signals through mammalian IP₃Rs.

Regulation by Ca²⁺

It has been demonstrated that cytoplasmic Ca²⁺ within the physiological range provides both positive and negative feedback for IP₃Rs and RyRs (Zucchi and Ronca-Testoni 1997; Bezprozvanny 2005; Foskett, et al. 2007). At low [Ca²⁺] the channel activity is potentiated, whereas it is inhibited at high Ca²⁺ concentrations. Several studies have documented that this biphasic Ca²⁺ regulation is a characteristic of IP₃Rs from different species representing insect, amphibian and mammalian IP₃Rs suggesting an evolutionary conserved mode of regulation (Bezprozvanny 2005; Foskett, et al. 2007). However, the underlying molecular mechanism is not clearly understood. Although in vitro studies have indicated that there are several putative Ca²⁺-binding sites scattered throughout the amino acid sequence of mammalian IP₃R1, their roles in mediating the receptor Ca²⁺ sensitivity are still largely

unknown (Sienaert, et al. 1997). Nevertheless, there is a well-conserved glutamate residue (E2100) in the regulatory domain and its mutation dramatically alters Ca²⁺ sensitivity of mammalian IP₃R (Tu, et al. 2003). Therefore, it has been proposed that this glutamate is critical for the Ca²⁺ sensor region of IP₃R. Interestingly, both *C. owczarzaki* IP₃R proteins contain a conserved glutamate residue homologous to the mammalian E2100 (supplementary fig. S3C, Supplementary Material online).

To determine whether CO.IP₃R-A is modulated by Ca²⁺ in a manner similar to mammalian receptors, IP₃-induced Ca²⁺ release was monitored in Mag-Fluo4-AM loaded DT40-3KO cells expressing CO.IP₃R-A or rIP₃R1 as described in the Materials and Methods. Ca²⁺ release was initiated by exposure to either 10 or 100 μM IP₃ in the presence of either 50 nM or 1 μM [Ca²⁺]. These [Ca²⁺] were chosen as representative of resting and maximally activated Ca²⁺ in mammalian cells. Figure 5A and C shows that the rate of rIP₃R1-mediated Ca²⁺ release was inhibited by reducing extracellular Ca²⁺, suggesting that Ca²⁺ is required for maximum channel activation consistent with previous findings (Zucchi and Ronca-Testoni 1997; Bezprozvanny 2005; Foskett, et al. 2007). However, under identical experimental conditions, Ca²⁺ release mediated by CO.IP₃R-A was not altered by the 20-fold change in [Ca²⁺] (fig. 5B and C). These data suggest that CO.IP₃R-A is not regulated by Ca²⁺, at least in an identical

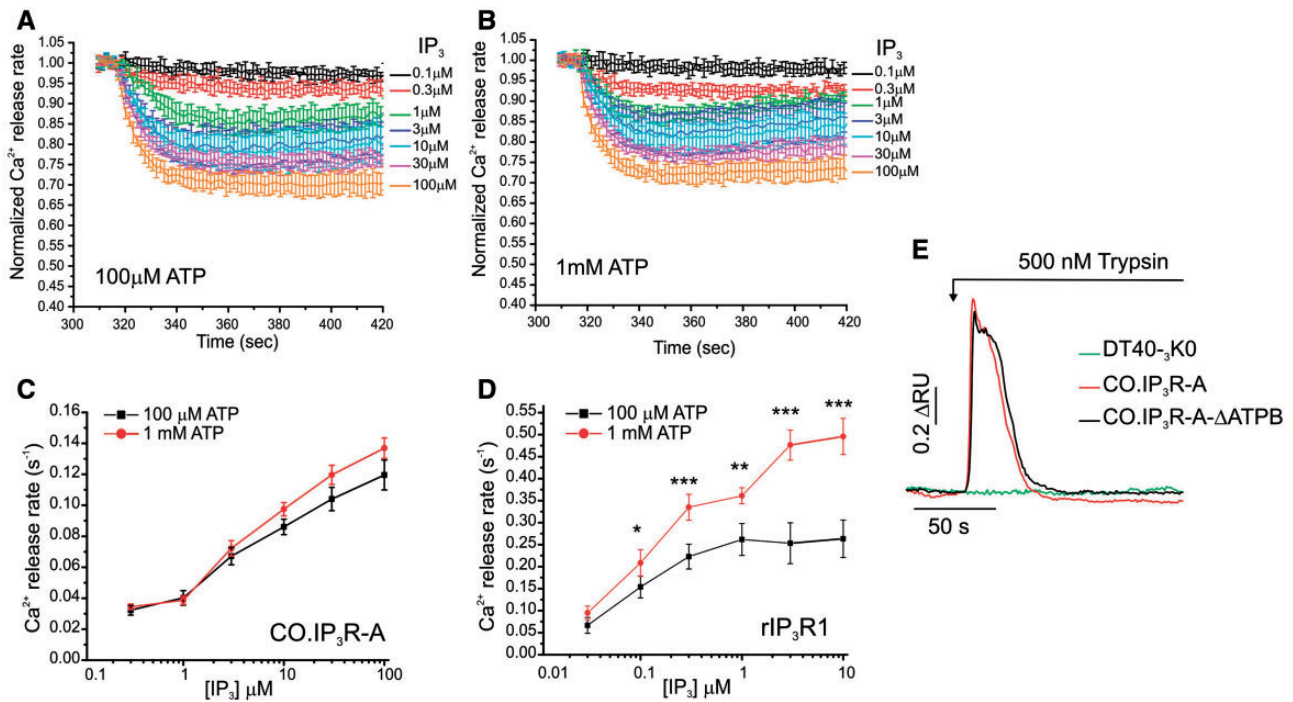


FIG. 6. Modulation of CO.IP₃R-A by ATP. (A, B) DT40.3KO expressing CO.IP₃R-A were loaded with Mag-Fluo4 and permeabilized. 100 μM ATP was added to activate SERCA pumps and fill intracellular calcium stores. Cells were then stimulated with the indicated concentrations of IP₃ in the presence of 100 μM (A) or 1 mM ATP (B). Fluorescence was normalized to the initial fluorescence intensity prior to release by IP₃. (C) Rate of calcium release calculated from experiments in (A) and (B) by fitting the average time courses from the first 30 s of IP₃ addition. (D) Rate of calcium release calculated from experiments using cells expressing rIP₃R1 performed as in (A)–(C). Rates were normalized to the maximum release rate. Three independent plates were used. (E) DT40-3KO or DT40-3KO stably expressing wild-type CO.IP₃R-A and CO.IP₃R-AΔATPB were loaded with Fura-2AM, and stimulated with 500 nM trypsin. Ca²⁺ release was measured as a change in the 340/380 fluorescence ratios. Ratio values were normalized to the initial baseline. Shown are representative traces.

manner to mammalian IP₃R. This appears to occur despite the fact that E2100 is conserved in mammalian and *Capsaspora* orthologs and thus suggests that the particular context of the binding motif is important. Further work will be necessary to determine whether CO.IP₃R-A is indeed absolutely refractory to modulation by Ca²⁺ or exhibits a shifted sensitivity reflecting the specific cellular environment of the organism.

Regulation by ATP

IP₃Rs expressed in mammalian, amphibian, and arthropod lineages are regulated by ATP (Bezprozvanny 2005; Foskett, et al. 2007; Yule, et al. 2010). It is thought that ATP binds to a glycine rich motif (GXGXXG) termed the Walker motif. Mammalian IP₃R1 contains two such motifs termed ATPA and ATPB. In addition, alternative splicing events can generate an additional glycine rich motif referred to as ATPC in IP₃R1 (Yule, et al. 2010). However, IP₃R2 and IP₃R3 contain sequences corresponding only to ATPB. It has been shown that although Ca²⁺ release by mammalian IP₃R1 and IP₃R3 is enhanced by ATP regardless of the IP₃ concentrations, IP₃R2 is regulated only at submaximum IP₃ concentrations (Yule, et al. 2010). CO.IP₃R-A has one putative ATP-binding site corresponding to the mammalian ATPB (supplementary fig. S3C, Supplementary Material online). To investigate whether ATP is required for CO.IP₃R-A activity, Ca²⁺ release was monitored

in permeabilized DT40-3KO cells expressing CO.IP₃R-A or rIP₃R1. Cells were loaded with Mag-Fluo4-AM. Ca²⁺ release was initiated by adding IP₃ in the absence or presence ATP. Figure 6A–C shows that Ca²⁺ release by CO.IP₃R-A was not potentiated in the presence of 1 mM ATP. However, rIP₃R1-mediated Ca²⁺ release was significantly enhanced by ATP, consistent with previous studies (fig. 6D) (Bezprozvanny 2005; Foskett, et al. 2007; Yule, et al. 2010). These data indicate that under our experimental conditions CO.IP₃R-A was not modulated by ATP, unlike mammalian IP₃Rs. To confirm that the putative ATP-binding motif is not required for Ca²⁺ release activity, the three glycines in the CO-IP₃R-A putative ATP binding (²³⁸⁸GLGLLG²³⁹³) were mutated to alanines. This mutation has been shown to completely abrogate nucleotide binding in mammalian IP₃Rs (Yule, et al. 2010). When cells expressing CO.IP₃R-A mutant (CO.IP₃R-A.ΔATPB) were stimulated with trypsin, robust Ca²⁺ release activity was initiated (fig. 6E). The amplitude of Ca²⁺ release was essentially identical to that mediated by wild-type CO.IP₃R-A (data not shown). These findings suggest that this glycine-rich motif sequence is not required for maximum CO.IP₃R-A activity.

Regulation by Cyclic AMP-Dependent Protein Kinase

Mammalian IP₃Rs are substrates for a wide variety of protein kinases (Vanderheyden, et al. 2009; Yule, et al. 2010). In general, protein phosphorylation can regulate protein

localization, activity, stability or its interaction with other proteins. PKA has been shown to enhance Ca²⁺ release activity of both IP₃R1 and IP₃R2 by phosphorylating these proteins at PKA consensus sites (Yule, et al. 2010). Scanning CO.IP₃R-A amino acid sequence for consensus PKA sites reveals a number of putative sites located in the C-terminal half of the protein (data not shown). Furthermore, the genome of *C. owczarzaki* contains several sequences that encode putative PKA-like proteins (Suga, et al. 2013). To investigate whether CO.IP₃R-A is regulated by PKA, DT40-3KO cells expressing CO.IP₃R-A or rIP₃R1 were loaded with Fura-2AM and loaded cells were preincubated with the adenylyl cyclase activator, forskolin, or the vehicle dimethyl sulphoxide (DMSO) DMSO. Figure 7A and B shows that PAR receptor-stimulated Ca²⁺ signals were significantly augmented by forskolin in cells expressing rIP₃R1 but not cells expressing CO.IP₃R-A (fig. 7C). These data demonstrate that under these conditions CO.IP₃R-A activity is not modulated by raising cellular cAMP or PKA activation.

Discussion

The ability to strictly regulate intracellular Ca²⁺ is essential to the growth, development, and survival of all living organisms (Plattner and Verkhatsky 2013). Eukaryotic cells are endowed with complex systems controlling Ca²⁺ entry and extrusion as well as sequestration in intracellular stores (Verkhatsky and Parpura 2014). Ca²⁺ flow from internal stores is regulated by two major intracellular release channel families, namely the IP₃Rs and RyRs (Fill and Copello 2002; Foskett, et al. 2007). Notably, members of IP₃R and RyR families are expressed differentially in different cell types and have distinct functional characteristics presumably suited to support the integrated cellular networks of multicellular species (Giannini, et al. 1995; Taylor, et al. 1999). Moreover, it is presumed that the evolution of these intracellular Ca²⁺ release channels coincided with the appearance of membrane-bound Ca²⁺ stores in early unicellular eukaryotes (Plattner and Verkhatsky 2013; Verkhatsky and Parpura 2014). However, the origin and history of IP₃R and RyR remains poorly defined. Nevertheless, it has recently been shown that many components of Ca²⁺ signaling machinery are encoded in the genomes of many unicellular eukaryotes (Cai 2008; Cai and Clapham 2008, 2012; Cai, et al. 2014). Whether, or how, unicellular IP₃R- and RyR-mediated signaling has contributed to the evolution and success of multicellular organisms is presently unknown.

In this report, we have used the available genomic and transcriptomic data from representative species along the eukaryotic tree of life and performed phylogenetic analyses to explore the origins of IP₃R and RyR. Our data suggest that the ancestral channels diverged into two paralogous families; IP₃R-A and IP₃R-B/RyR at the dawn of Opisthokonta. At the stem of Holozoa, IP₃R-B/RyR gave rise to IP₃R-B and RyR. The signaling innovations associated with the holozoan origin were correlated with duplication of IP₃R-A and RyR genes and loss of IP₃R-B in vertebrates. However, the wide-spread occurrence of IP₃R-B alongside IP₃R-A suggests that IP₃R-B may as well have vital biological functions in these extant

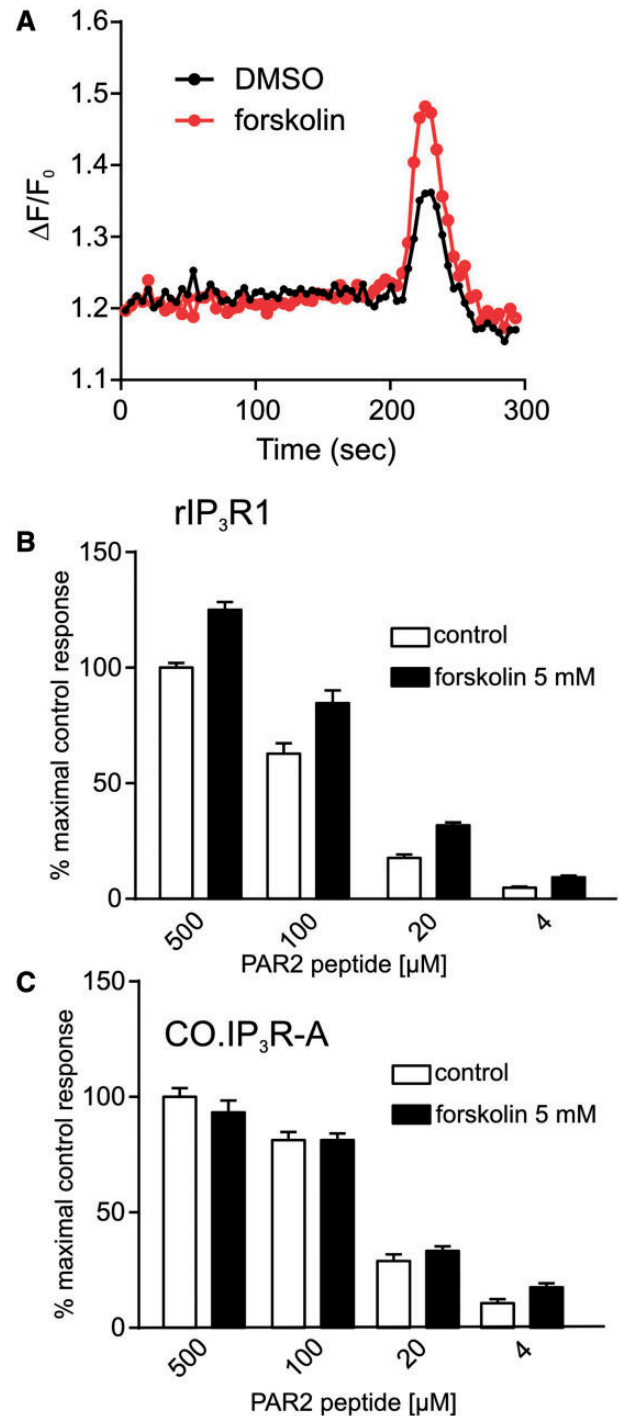


Fig. 7. Modulation of CO.IP₃R-A by cyclic AMP-dependent protein kinase. (A) DT40.3KO expressing rIP₃R1 were loaded with Fura-2AM and plated into a 0.1% (w/v) polylysine coated 96-well plate. Cells were preincubated with 5 μM forskolin or DMSO followed by the addition of the indicated amounts of PAR peptide to activate PAR receptor. Ca²⁺ traces were acquired and analyzed using SoftMax Pro Microplate Software. Peak fluorescence for each well was normalized to the baseline fluorescence and was expressed as a percentage of the control maximum. Representative traces are shown. (B) Quantification of Ca²⁺ release expressed as percent of maximum release in cells expressing rIP₃R1 in response to different PAR peptide concentrations. (C) Quantification of Ca²⁺ release expressed as percent of maximum release in cells expressing CO.IP₃R-A treated as in the (A) and (B).

species. Indeed, the specific pattern of gene regulation of CO.IP₃R-B in *C. owczarzaki* and the indication that this protein may be regulated very differently from CO.IP₃R-A suggests distinct function for this protein.

The phylogenetic tree presented here indicates that the IP₃R/RyR gene family is present in almost all known eukaryotes and is consistent with the view that this gene family is pivotal for the adaptation required for the eukaryotic life style. It is not clear why and how some eukaryotic taxa such as terrestrial plants and most fungi do not contain any recognizable IP₃R/RyR gene. Nevertheless, the inability to identify IP₃R/RyR genes in plants and fungi might be due to substantial divergence of these genes or incorporation of protein domains by horizontal gene transfer. Indeed, recent studies have shown that both plant and yeast cells exhibit IP₃-evoked Ca²⁺ release suggesting the presence of IP₃-sensing Ca²⁺ releasing channels (Tisi, et al. 2004; Krinke, et al. 2007). Intriguingly, our phylogenetic analyses provide tantalizing evidence that IP₃R genes and thus IP₃-induced Ca²⁺ signaling predate RyR genes.

As an exemplar of a premetazoan species we investigated the Ca²⁺ signaling machinery of *C. owczarzaki*. It appears that *C. owczarzaki* encodes two IP₃R orthologs and one RyR, together with several other proteins associated with Ca²⁺ signaling. Our findings demonstrate that CO.IP₃R-A, CO.IP₃R-B, and RyR are expressed in *C. owczarzaki* and are differentially regulated both in various stages of *C. owczarzaki* life cycle and under different growth conditions. This suggests that it employs different components of its Ca²⁺ signaling machinery to meet metabolic and environmental challenges. Amino acid sequence analyses of CO.IP₃R-A and CO.IP₃R-B revealed a conservation of many motifs characteristics of “modern” IP₃Rs. We cloned CO.IP₃R-A and CO.IP₃R-B and expressed them in a heterologous cell system. Although the two *C. owczarzaki* proteins appear to be targeted to the ER, coimmunoprecipitation experiments indicate that CO.IP₃R-A and CO.IP₃R-B do not associate with each other and thus do not form heteromeric channels. CO.IP₃R-A association with rIP₃R1 suggests that oligomerization interfaces are highly conserved. These results indicate conserved molecular function between *C. owczarzaki* and mammalian IP₃R-A and, at the same time, suggest profound functional differences between IP₃R-A and IP₃R-B.

Furthermore, our data reveal that CO.IP₃R-A behaves like a canonical IP₃R in some respects. For example, CO.IP₃R-A binds IP₃ and is competent to mediate IP₃-evoked Ca²⁺ release. In addition, although the potential impact on *C. owczarzaki* is beyond the scope of this study, based on the motif predicted to form the putative pore, Ca²⁺ flux through the pore of CO.IP₃R-A would be predicted to be greater than mammalian IP₃R (Gao, et al. 2000; Boehning, et al. 2001). On the other hand, CO.IP₃R-B does not bind IP₃ and does not mediate Ca²⁺ release. That CO.IP₃R-B does not support Ca²⁺ release may be explained by divergence in the primary amino acid sequence at regions crucial for function. First, CO.IP₃R-B lacks three of the ten conserved basic residues that have been shown to be critical for IP₃ binding and consistent with this it does not bind IP₃ (Yoshikawa, et al. 1996). Second, CO.IP₃R-B would be predicted to exhibit altered ion

permeability as the sequence corresponding to the selectivity filter is highly divergent and in fact has few similarities to any known ion channels. However, it appears from our analysis and published reports that multiple conserved motifs are necessary for IP₃-gated Ca²⁺ channel activity. For example, although CO.IP₃R-B is not functional in DT40 cells, previous studies have shown that IP₃Rs from *T. brucei* and *T. cruzi* are functional when expressed in this system (Hashimoto, et al. 2013; Huang, et al. 2013). *Trypanosoma* IP₃Rs lack many conserved residues in their respective ligand-binding domains however, as with mammalian IP₃R and CO.IP₃R-A they have a recognizable selectivity filter motif. Although the function of CO.IP₃R-B is unclear, it is tempting to speculate that CO.IP₃R-B may retain some of the other properties associated with mammalian IP₃R-A family proteins. This might include acting as a scaffold for signaling protein complexes. Furthermore, given that mammalian intracellular Ca²⁺ channel activity is modulated by a large number of cellular events including redox state, the cytoplasmic ionic milieu, accessory proteins, and many posttranslational modifications, it is possible that CO-IP₃R-B is specialized in the organisms that express these proteins, to signal by predominately responding to alternative factors other than changes in IP₃.

It is presumed that IP₃R serves as a signal integrator whereby input from extracellular and intracellular stimuli is converted into a Ca²⁺ signal with specific temporal and spatial properties (Berridge, et al. 2000; Berridge, et al. 2003; Foskett, et al. 2007). This signal is, in turn, utilized to evoke a specific biological response. In part, this is accomplished by modulating IP₃R channel activity. In many animal systems, IP₃R activity is modulated by the cellular pool of nucleotides, reactive oxygen species, intracellular [Ca²⁺], phosphorylation, and protein–protein interactions (Bezprozvanny 2005; Foskett, et al. 2007; Yule, et al. 2010). As the IP₃R molecule is a premetazoan innovation, we investigated whether important representative routes of regulation of IP₃R are unique to multicellular organisms. Experiments were conducted to investigate the regulatory activity of [ATP], [Ca²⁺], and phosphorylation by PKA. Somewhat surprisingly, our data show that although these events had predictable effects on rIP₃R1, the activity of CO.IP₃R-A was unaffected. This might suggest that regulation of IP₃R by these factors is a metazoan sophistication, necessary for maintaining signal fidelity in an environment where more Ca²⁺ effectors and regulated processes have evolved. Nevertheless, a caveat associated with these experiments is that the concentrations of Ca²⁺ or ATP used in our assays might be beyond the physiological threshold in which CO.IP₃R-A is most responsive. Further, CO.IP₃R-A phosphorylation by PKA might not lead to potentiation of the channel activity but to some other regulatory outcome not detected by our assay protocol.

In conclusion, our findings are consistent with the notion that IP₃R-A, IP₃R-B, and RyR gene families evolved before the rise of multicellularity. Our data suggest that although CO.IP₃R-A is gated by IP₃ and thus exhibits basic functionality, it is not regulated by common cellular signals known to regulate IP₃Rs in different multicellular species. Thus, CO.IP₃R-A, and perhaps ancient unicellular IP₃Rs, might be functionally

“less multifaceted” than the metazoan counterparts. The developmental and physiological requirements of multicellular organisms might have necessitated an increase in the IP₃R responsiveness to internal and external metabolic signals. Future studies are required to investigate the regulation of IP₃R-mediated Ca²⁺ signaling in *C. owczarzaki* cells and other unicellular species.

Materials and Methods

Reagents

Restriction enzymes were from New England Biolabs. *Pfu* Ultra II Hotstart 2X Master Mix was from Agilent. PrimerScript First Strand cDNA synthesis kit was from TaKaRa. Clone ID 1X Colony PCR Master Mix was from Lucigen. Peptone was obtained from Bacto. Yeast extract was from BD Transduction laboratories. KH₂PO₄, Na₂HPO₄, yeast nucleic acid, folic acid, hemin, and monoclonal anti-Flag M2 antibody were from Sigma. HA.11 monoclonal antibody was purchased from Covance. Fetal bovine serum was from Gemini Bio-products. T4 ligase and Dylight 700CW and Dylight 800CW secondary antibodies were from Thermo Scientific. Protein A/G Plus-agarose was from Santa Cruz Biotechnology. DMEM (Dulbecco's modified Eagle medium), Roswell Park Memorial Institute (RPMI) 1640 media, chicken serum, beta mercaptoethanol, G418 sulfate, and Trizol were from Invitrogen. Reagents used for sodium dodecyl sulfate polyacrylamide gel electrophoresis (SDS-PAGE) were purchased from Bio-Rad.

Phylogenetic Analyses

IP₃R sequences were searched in complete genome or transcriptome sequences of 102 taxa representing all known eukaryotic supergroups. Taxon sampling included 20 animals, 10 unicellular holozoans, 26 fungi, 2 nucleariids, 1 apusozoan, 4 amoebozoans, 7 plants, 5 chlorophytes, 3 rhodophytes, 9 heterokonts, 5 alveolates, 2 rhizarians, 1 haptophyte, 1 cryptophyte, and 6 excavates (supplementary table S1, Supplementary Material online). The identification of IP₃R sequences in all these species was done using HMMER (Eddy 1998), searching with the hmm profiles of three Pfam domains found in canonical IP₃R: Ins145_P3_rec domain (PF08709), RIH_assoc domain (PF08454), and RYDR_ITPR domain (PF01365). This was in order to maximize the identification of partial sequences, which may contain only one of these domains. A fasta file with all the identified sequences (removing those redundantly found in the three HMMER searches) is included in supplementary file S1, Supplementary Material online. The identified sequences were aligned using the Mafft L-INS-i algorithm, optimized for local sequence homology (Kato, et al. 2002), and manually inspected and edited. This resulted in a matrix containing 332 amino acid residues. Extremely diverging sequences were removed from the alignment.

Maximum-likelihood phylogenetic trees were estimated by RaxML (Stamatakis 2006) using the PROTGAMMALG model, which uses the Le and Gascuel (LG) model of evolution (Le and Gascuel 2008) and accounts for between-site rate

variation with a four-category discrete gamma approximation (LG+Γ). Statistical support for bipartitions was estimated by performing 100-bootstrap replicates using RaxML with the same model. Bayesian inference trees were calculated with PhyloBayes 3.3 (Lartillot, et al. 2009) using two parallel runs for 500,000 generations and sampling every 100 and with the LG+Γ model of evolution. Bayesian posterior probabilities were used for assessing the statistical support of each bipartition.

Capsaspora owczarzaki Culture and Maintenance

Capsaspora owczarzaki cells were maintained in ATCC medium 1034 (Modified PYNFH medium). To make 1 l of complete medium, 10 g peptone, 10 g yeast extract, 1 g yeast nucleic acid, 15 mg folic acid, and 1 mg hemin were dissolved in 880 ml distilled H₂O. After adjusting the pH to 6.5, the solution was sterilized by autoclaving at 121 °C for 15 min. Before use, 100 ml of Fetal Bovine Serum (FBS) and 20 ml of buffer solution (18.1 g KH₂PO₄ and 25 g of Na₂HPO₄ dissolved in 1 l distilled water and filter-sterilized) were added.

Semiquantitative RT-PCR

Capsaspora owczarzaki were grown in normal growth media or under nutrient deprivation and were harvested 24 h later. Total RNA was isolated using TRIzol (Invitrogen) following the manufacturer's instructions. To avoid amplifying any contaminating traces of genomic DNA, total RNA was treated with DNA-free kit (Ambion). RNA was then used for first strand synthesis using SuperScript Reverse Transcriptase III (Invitrogen) according to the manufacturer's protocol. The relative transcriptional levels were determined using equal amounts of cDNA and gene specific primers. PCR reactions were carried out using Clone ID polymerase reaction mix and were terminated during the exponential phase of the amplification. The primers are shown in supplementary table S3, Supplementary Material online. GAPDH was used as a control.

RNA Sequencing

The expression profiling and analyses were performed as described previously (Sebe-Pedros, et al. 2013). In short, RNA was extracted from three biological replicates of each of the life stages of *C. owczarzaki*, using Trizol reagent. Strand-specific libraries were prepared and sequenced with HiSeq 2000 instrument (Illumina, San Diego, CA). Reads were aligned to the reference genome using Tophat (Trapnell, et al. 2012) with default options. Significant differential expression was calculated by performing pairwise comparisons with DESeq (Anders and Huber 2010) (threshold 1 e-05), EdgeR (Robinson, et al. 2010) (threshold 1 e-05), CuffDiff (Trapnell, et al. 2012) (threshold 1 e-05), and NOISeq (threshold 0.8) and only genes that appear to be significant at least in three out of the four methods were considered as differentially expressed.

Cloning of CO.IP₃R-A

Capsaspora owczarzaki cells growing in axenic conditions were harvested by centrifugation and total RNA was isolated using Trizol following manufacturer's protocol. cDNA was made using PrimerScript First Strand cDNA synthesis kit. Cloning of CO.IP₃R-A was made at two steps and using primers based on genomic data deposited in the Origins of Multicellularity Database. A forward primer: (GATTATCGA GATTCTCGAATTCATCAGCGATGTTCCGGCTCGACTTTCGC) (underlined is *Eco*RI site) and reverse primer: (gcttctagagcggcgcCTAATCGTCAGCAGAAATCAGACTGTTCCGGTTGCTGGAAGG) (*Not*I site underlined, stop codon in bold) were used to amplify 6.2 kb corresponding to the C-terminal part of the coding region of CO.IP₃R-A. PCR product was digested with *Eco*RI and *Not*I and the *Eco*RI–*Not*I fragment was inserted into corresponding sites in pEGFP-N1 (Clontech) to create 6.2 pN1 with Enhanced Green Fluorescent Protein (EGFP) deleted in this process. The 3.4 kb corresponding to the N-terminal fragment of the coding sequence was amplified using forward primer: (TACGTAGCTAGCGCCAGCATGAGCTCGCCTCGTTACTTGCGGCTCGGCGATGTCGTGTC) which contains *Nhe*I site (underlined) and Kozak sequence (in italic) in the context of the start codon (in bold) to enhance expression, and reverse primer (GCGAAAGTCGAGCCGAACATCGCTGATGAATTCGAGAATCTCGATAATC) (*Eco*RI site underlined). The amplified fragment was digested with *Nhe*I and *Eco*RI and inserted into correspondingly cut 6.2pN1 plasmid to obtain a plasmid encoding the entire coding sequence. This construct was further modified to insert a flag tag immediately after the initiation methionine using a pair of primers: forward (CCGCTAGCGCCACCATGGATTACAAGGATGACGATGACAAGAGCTCGCTCGTTAC) and reverse (GTAACGAGGCGAGCTCTTGT CATCGTCATCCTTGTAATCCATGGTGGCGCTAGCGG). To create HA-tagged protein, the C-terminal end of the protein was modified using forward: (CTGCTGACGATTAC CCA TAC GAC GTC CCA GAC TAC GCTTAGGCGGCCGCGAC TC) and reverse: (GAGTCGCGGCCGCTAAGCGTAGTCTGGACGTCGTATGGTAATCGTCAGCAG). To construct mCherry fusion protein, QuikChange mutagenesis was carried out to engineer *Xba*I site just before the stop codon using forward: (GATTTCTGCTGACGAtgcTCTAGATAGcGGCCGACTCTAG) and reverse: (CTAGAGTCGCGGCCgcCTATCTAGAgcaTCGTCAGCAGAAATC). Two extra nucleotides were included so that the coding sequence is inframe with mCherry protein. pmCherry-C1 (Clontech) was digested with *Nhe*I and *Xba*I, and the *Nhe*I–*Xba*I fragment encompassing mCherry coding region was inserted into *Xba*I site engineered after CO.IP₃R-A coding sequence (*Nhe*I and *Xba*I have compatible sticky ends). Finally, to create CO.IP₃R-AΔATP, QuikChange mutagenesis protocol was used to mutate three glycine into alanine in the potential ATP-binding site (²³⁸⁸GLLLG²³⁹³) using forward: (CTCGACCTCGGGCGCGCTCGCTCTGCTTGCTTGTtATCAAC) and reverse: (GTTGATaACAAGGCAAGCAGAGCGGAGCGCCCCGAGGTCGAG) (*Bss*HI site underlined, introduced

to facilitate screening). All constructs were verified by sequencing.

Cloning of CO.IP₃R-B

Two primers were used to amplify 2.6 kb coding for the most C-terminal region of the coding sequence using forward (GGCACAAGGAATTCAGCGCTCGTTTGAAAAGTTCT) which contains an *Eco*RI site (bold) and *Afe*I site (underlined) and reverse (GCTTCTAGAGCGGCCGCTTAACGCCTGGCAGCAGTGCGC) (*Not*I site underlined). The amplified fragment was then digested with *Eco*RI and *Not*I site, gel-extracted, and inserted into correspondingly digested pEGFP-N1 to generate 2.6pN1 with EGFP deleted in this process. The 5-kb fragment corresponding to the N-terminal part of the gene was amplified using two primers: Forward (TACGTAGCTAGCGCCAGCATGCCGCTGTCGCCAAGACCAAGAAGGGC), which contains *Nhe*I site (underlined) and reverse primer (CAAAAAGAAGAATTCAAACGAGCGCTGGACTTCCTTGTTG), which contains *Eco*RI site (bold) and *Afe*I site (underlined). The PCR product was digested with *Nhe*I and *Afe*I and the purified product was inserted into *Nhe*I and *Afe*I sites of 2.6pN1 to create 7.6pN1 construct. The 277 bp coding for the first 89 amino acids was synthesized by GenScript and it was flanked by *Nhe*I sites. The pUC57 vector containing 227 bp was digested with *Nhe*I, and the fragment purified and inserted into correspondingly digested 7.6pN1 construct. To remove extranucleotides added during this process, the resultant construct was further modified using forward (CCA GGCTCTCAAGAAGAAAATGCCGCTGTCGCCAAGACCAAG) and reverse (CTTGGTCTTGGCGACAGCCGGCATTCTTCTTCTGAGAGCCTGG). To make HA-tagged CO.IP₃R-B, the following primers were used to modify the 3'-end: Forward (CACTGCTGCCAGGCGTTACCCATACGACGTCCAGACTACGCTTAAGCGGCCGCGACTC) and reverse (TCTAGAGTCGCGGCGCTTAAGCGTAGTCTGGGACGTCGTATGGGTAACGCC TGGCAGC). Finally, CO.IP₃R-B mCherry fusion protein was constructed by inserting an *Xba*I site just before the stop codon using a primer pair: Forward (GCTGCCAGGCGTCTA GATAAGCGGCCGCGACTCTAG) and reverse (CTAGAGTCGC GGCCGCTTATCTAGACGCTGGCAGC). pmCherry-C1 was digested with *Nhe*I and *Psp*OMI and the *Nhe*I–*Psp*OMI fragment encompassing mCherry coding region was inserted into *Xba*I–*Not*I sites after CO.IP₃R-B coding sequence (*Not*I and *Psp*OMI have compatible cohesive ends). All constructs were verified by sequencing.

Vertebrate Cell Culture and Transfection

DT40-3KO cell line, chicken B-lymphoid cell devoid of the three endogenous IP₃R isoforms, was maintained in RPMI supplemented with 1% chicken serum, 10% fetal bovine serum, 100 units/ml penicillin, 100 μg/ml streptomycin at 39 °C, and 5%CO₂. Cells were subcultured every 3 days. Transfection and generation of stable cell line were performed as described before (Alzayady, et al. 2013). Briefly, plasmids coding for rat IP₃R1 (rIP₃R1), CO.IP₃R-A, and CO.IP₃R-B were linearized with *Nru*I, *Ase*I, and *Afl*II, respectively. Five million

cells were pelleted by centrifugation and washed once with phosphate-buffered saline (PBS) and then electroporated with 5–10 µg of linearized plasmid using Amaxa cell nucleofector kit T (Lonza Laboratories). Cells were supplied with fresh complete media and allowed to recover for 24 h before passaging into media containing 2 mg/ml G418 in five 96-well plates. Immunoblot analyses were used to screen G418-resistant clones for expression of the desired constructs after 10–14 days.

HEK293 cells were grown at 37 °C, 5% CO₂ in DMEM supplemented with 100 units/ml penicillin, 100 µg/ml streptomycin, and 10% fetal bovine serum. For transfection, HEK293 cells were seeded at 500,000 cells per well in 6-well plates. Cells were transfected next day with cDNA constructs using lipofectamine2000 following the manufacturer's protocol. Cells were harvested 24–48 h after transfection.

Cell Lysates and SDS-PAGE

Cells expressing the desired constructs were harvested by centrifugation, washed once with PBS and lysed in Triton X-100 lysis buffer (1% Triton X-100, 150 mM NaCl, 50 mM Tris base, 1 mM ethylenediaminetetraacetic acid [EDTA], pH8) supplemented with protease inhibitors (Roche). Lysates were incubated on ice for 30 min with occasional vortexing and were then cleared by centrifugation at 16,000 × g for 10 min at 4 °C. Cleared lysates were transferred into fresh tubes and protein concentrations were determined using D_c protein assay kit (Bio-Rad). Proteins were fractionated on SDS-PAGE, electroblotted on nitrocellulose and probed with the indicated antibodies. Odyssey infrared imaging system (LI-COR Biosciences) was used to visualize and quantify protein bands.

Coimmunoprecipitation

HEK293 cells were cotransfected with the desired constructs as described above. Forty-eight hours posttransfection, cells were collected by scraping in PBS and pelleted by centrifugation. Cell pellets were washed once with PBS and lysed in Igepal lysis buffer containing: 120 mM NaCl, 50 mM Tris-HCl, 0.5% Igepal (v/v), 1 mM EDTA, plus a tablet of protease inhibitor cocktail. After clearing the lysates, proteins were immunoprecipitated overnight with the desired antibodies plus protein A/G agarose beads. Immunocomplexes were washed four times with lysis buffer and resuspended in gel loading buffer, fractionated on 5% SDS-PAGE, and processed in immunoblots using the indicated antibodies. The efficiency of coimmunoprecipitation was expressed as the relative amount of coimmunoprecipitated proteins normalized to the amounts of the same proteins in the lysates and this value was divided by the amount of the immunoprecipitated proteins.

Confocal Fluorescent Microscopy

To examine protein subcellular localization, the HEK293 cells were cultured on 25-mm glass coverslips in 6-well plates and transiently cotransfected with various mCherry-fusion constructs along without or with UBC6-ER targeting sequence tagged with Venus fluorescent protein (a kind gift from P.

Kammermeier, University of Rochester). 24–48 h later, cells were washed twice with PBS and fixed with methanol for 2 min at room temperature. Coverslips were then washed four times with PBS and mounted on glass slide using mounting media. Cells were visualized using an Olympus FluoView1000 confocal microscopy equipped with a suite of gas and diode lasers.

Sequence Alignment and Structural Analyses

Sequence alignment was created using the Clustal Omega Multiple sequence alignment program. Amino acid sequence identity and similarity were calculated using Webserver bioninformatics.org. Signature motifs were identified by visual inspection.

IP₃-Binding Assay

DT40.3KO cells expressing HA-tagged CO.IP₃R-A or CO.IP₃R-B were grown in T75 flasks until confluence. Cells were then harvested by centrifugation and lysed in Triton X-100 lysis buffer supplemented with a tablet of protease inhibitor cocktails. After clearing the lysates, proteins were immunoprecipitated overnight with HA.11 antibodies and immunocomplexes were captured with protein A/G agarose beads. Immunocomplexes were washed four times with lysis buffer and once with IP₃-binding buffer (50 mM Tris-base, 1 mM EDTA, 1 mM betamercaptoethanol pH8). The binding reaction was performed in 100 µl volume containing 2.5 nM tritiated IP₃ (³H-IP₃) and increasing concentrations of cold IP₃ at 4 °C for 1 h. At the end of the incubation period, beads were pelleted by centrifugation at 13,000 × g and supernatants were removed. Afterwards, 500 l of 1% of SDS was added to each tube and tubes were left at room temperature overnight on the bench. Next day, tube contents were transferred to scintillation vials and 4 ml of scintillation liquid was added to each vial. Bound radioactivity was measured in a liquid scintillation counter. Nonspecific binding is defined as the amount of bound radioactivity in the presence of 50 µM cold IP₃. Specific binding is determined by subtracting the count per minute (CPM) values obtained in the presence of 50 µM cold from the CPM values obtained with other conditions. Total specific binding is specific binding in the absence of cold IP₃. All values were normalized to total specific binding. Normalized specific binding from three to four experiments was averaged and SE was determined. Fitting curves were generated using averaged normalized specific binding values.

Cytosolic Ca²⁺ Measurement

Single Cell Imaging

Cytosolic Ca²⁺ changes were measured as described before (Alzayady, et al. 2013). Briefly, DT40 cells were pelleted by centrifugation and washed once with imaging buffer (137 mM NaCl, 5.5 mM glucose, 0.56 mM MgCl₂, 4.7 mM KCl, 1.26 mM Ca²⁺, 10 mM HEPES, 1 mM Na₂HPO₄ at pH7.4). Cells were then loaded with 2 µM Fura2-AM and were allowed to attach to a glass coverslip mounted on

Werner chamber for 20 min at room temperature. Afterwards, loaded cells were perfused with imaging buffer and stimulated with the desired agonists at the indicated time points. TILLvisION software was used for image acquisition and analyses. Experiments were repeated at least three times.

FlexStation 3 Microplate Reader

DT40-3KO cells expressing the desired constructs were washed with imaging buffer containing 0.1% BSA and then loaded with 5 μ M Fura-2AM at room temperature for 60 min. Loaded cells were then washed and resuspended in imaging buffer containing 0.1% BSA and transferred into a 0.1% (w/v) polylysine coated 96-well plate. Cells were preincubated with 5 μ M forskolin or DMSO followed by the addition of the PAR2 peptide to activate PAR and generate IP₃. Fluorescence changes were measured with FlexStation 3 (Molecular Devices) and analyzed by using SoftMax Pro Microplate Data Acquisition & Analysis Software.

Permeabilized Cell Assays

DT40-3KO cells stably expressing the desired constructs were washed twice with imaging buffer and incubated with 20 μ M Mag-Fluo4-AM for 1 h at room temperature. Cells were then washed, resuspended in Ca²⁺ free media (140 mM KCl, 20 mM NaCl, 20 mM PIPES, 1 mM EGTA, and 2 mM MgCl₂, pH7.0) and permeabilized using 10 μ g/ml saponin. Permeabilization was confirmed by trypan blue accumulation. To investigate the requirement of Ca²⁺ for IP₃R1 activity, the permeabilized cells were washed and resuspended in Mg²⁺ free media (140 mM KCl, 20 mM NaCl, 20 mM PIPES, 300 μ M EGTA, 220 μ M CaCl₂, pH7.0) with a free [Ca²⁺] of 1 μ M. Cells were then dispersed into a black-walled flat bottom 96-well plates (500,000 cells/well) and spun to plate cells to the bottom of each well. Imaging was carried out using FlexStation 3 (excitation 490 nm, emission 525 nm). Briefly, stores were loaded by adding 1.5 mM Mg-ATP to activate SERCA. Upon loading, SERCA was disabled using cyclopiazonic acid and free [Ca²⁺] was either maintained at 1 μ M or reduced to 50 nM by the addition of BAPTA. IP₃Rs were then activated at the indicated [IP₃] in the presence of 5 mM ATP.

To assess the influence of ATP on IP₃R1 activity, after permeabilization, the cells were washed and resuspended in Mg²⁺ free media (140 mM KCl, 20 mM NaCl, 20 mM PIPES, 1 mM EGTA, 375 μ M CaCl₂, pH 7.0) with a free [Ca²⁺] of 300 nM. Cells were then dispersed into a black-walled flat bottom 96-well plates (500,000 cells/well) and spun to plate cells to the bottom of each well. Imaging was carried out using a FlexStation 3 (excitation 490 nm, emission 525 nm). Briefly, stores were loaded by adding 100 μ M Mg-ATP to activate SERCA. Upon loading, SERCA was disabled using cyclopiazonic acid and [ATP] was either maintained at 100 μ M or increased to 1 mM. IP₃Rs were then activated at determined [IP₃] at 300 nM [Ca²⁺].

Supplementary Material

Supplementary file S1, figures S1–S5, and tables S1–S3 are available at *Molecular Biology and Evolution* online (<http://www.mbe.oxfordjournals.org/>).

Acknowledgments

The authors are grateful to members of the Yule laboratory for many fruitful discussions. This work was supported in part by National Institute of Health grants RO1-DE14756 and RO1-DE19245 and by a grant (ERC-2013-CoG #616960) from the European Research Council to I.R.-T.

References

- Alzayady KJ, Wagner LE 2nd, Chandrasekhar R, Monteagudo A, Godiska R, Tall GG, Joseph SK, Yule DI. 2013. Functional inositol 1,4,5-trisphosphate receptors assembled from concatenated homo- and heteromeric subunits. *J Biol Chem*. 288:29772–29784.
- Anders S, Huber W. 2010. Differential expression analysis for sequence count data. *Genome Biol*. 11:R106.
- Berridge MJ, Bootman MD, Roderick HL. 2003. Calcium signalling: dynamics, homeostasis and remodelling. *Nat Rev Mol Cell Biol*. 4: 517–529.
- Berridge MJ, Lipp P, Bootman MD. 2000. The versatility and universality of calcium signalling. *Nat Rev Mol Cell Biol*. 1:11–21.
- Betzenhauser MJ, Marks AR. 2010. Ryanodine receptor channelopathies. *Pflugers Arch*. 460:467–480.
- Bezprozvanny I. 2005. The inositol 1,4,5-trisphosphate receptors. *Cell Calcium* 38:261–272.
- Bezprozvanny I. 2011. Role of inositol 1,4,5-trisphosphate receptors in pathogenesis of Huntington's disease and spinocerebellar ataxias. *Neurochem Res*. 36:1186–1197.
- Boehning D, Mak DO, Foskett JK, Joseph SK. 2001. Molecular determinants of ion permeation and selectivity in inositol 1,4,5-trisphosphate receptor Ca²⁺ channels. *J Biol Chem*. 276: 13509–13512.
- Brini M, Cali T, Ottolini D, Carafoli E. 2012. Calcium pumps: why so many? . *Compr Physiol*. 2:1045–1060.
- Cai X. 2008. Unicellular Ca²⁺ signaling “toolkit” at the origin of metazoa. *Mol Biol Evol*. 25:1357–1361.
- Cai X, Clapham DE. 2012. Ancestral Ca²⁺ signaling machinery in early animal and fungal evolution. *Mol Biol Evol*. 29:91–100.
- Cai X, Clapham DE. 2008. Evolutionary genomics reveals lineage-specific gene loss and rapid evolution of a sperm-specific ion channel complex: CatSpers and CatSperbeta. *PLoS One* 3:e3569.
- Cai X, Wang X, Clapham DE. 2014. Early evolution of the eukaryotic Ca²⁺ signaling machinery: conservation of the CatSper channel complex. *Mol Biol Evol*. 31:2735–2740.
- Case RM, Eisner D, Gurney A, Jones O, Muallem S, Verkhatsky A. 2007. Evolution of calcium homeostasis: from birth of the first cell to an omnipresent signalling system. *Cell Calcium* 42:345–350.
- Catterall WA. 2000. Structure and regulation of voltage-gated Ca²⁺ channels. *Annu Rev Cell Dev Biol*. 16:521–555.
- Clapham DE. 2007. Calcium signaling. *Cell* 131:1047–1058.
- Cui J, Matkovich SJ, deSouza N, Li S, Roseblit N, Marks AR. 2004. Regulation of the type 1 inositol 1,4,5-trisphosphate receptor by phosphorylation at tyrosine 353. *J Biol Chem*. 279:16311–16316.
- Derelle R, Lang BF. 2012. Rooting the eukaryotic tree with mitochondrial and bacterial proteins. *Mol Biol Evol*. 29:1277–1289.
- Eddy SR. 1998. Profile hidden Markov models. *Bioinformatics* 14: 755–763.
- Fairclough SR, Chen Z, Kramer E, Zeng Q, Young S, Robertson HM, Begovic E, Richter DJ, Russ C, Westbrook MJ, et al. 2013. Premetazoan genome evolution and the regulation of cell differentiation in the choanoflagellate *Salpingoeca rosetta*. *Genome Biol*. 14: R15.

- Fill M, Copello JA. 2002. Ryanodine receptor calcium release channels. *Physiol Rev.* 82:893–922.
- Foskett JK, White C, Cheung KH, Mak DO. 2007. Inositol trisphosphate receptor Ca²⁺ release channels. *Physiol Rev.* 87:593–658.
- Futatsugi A, Nakamura T, Yamada MK, Ebisui E, Nakamura K, Uchida K, Kitaguchi T, Takahashi-Iwanaga H, Noda T, Aruga J, et al. 2005. IP3 receptor types 2 and 3 mediate exocrine secretion underlying energy metabolism. *Science* 309:2232–2234.
- Gao L, Balshaw D, Xu L, Tripathy A, Xin C, Meissner G. 2000. Evidence for a role of the luminal M3-M4 loop in skeletal muscle Ca(2+) release channel (ryanodine receptor) activity and conductance. *Biophys J.* 79:828–840.
- Gees M, Colsoul B, Nilius B. 2010. The role of transient receptor potential cation channels in Ca²⁺ signaling. *Cold Spring Harb Perspect Biol.* 2: a003962.
- Giannini G, Conti A, Mammarella S, Scrobogna M, Sorrentino V. 1995. The ryanodine receptor/calcium channel genes are widely and differentially expressed in murine brain and peripheral tissues. *J Cell Biol.* 128:893–904.
- Hashimoto M, Enomoto M, Morales J, Kurebayashi N, Sakurai T, Hashimoto T, Nara T, Mikoshiba K. 2013. Inositol 1,4,5-trisphosphate receptor regulates replication, differentiation, infectivity and virulence of the parasitic protist *Trypanosoma cruzi*. *Mol Microbiol.* 87: 1133–1150.
- He D, Fiz-Palacios O, Fu CJ, Fehling J, Tsai CC, Baldauf SL. 2014. An alternative root for the eukaryote tree of life. *Curr Biol.* 24:465–470.
- Hertel LA, Bayne CJ, Loker ES. 2002. The symbiont *Capsaspora owczarzaki*, nov. gen. nov. sp., isolated from three strains of the pulmonate snail *Biomphalaria glabrata* is related to members of the Mesomycetozoa. *Int J Parasitol.* 32:1183–1191.
- Huang G, Bartlett PJ, Thomas AP, Moreno SN, Docampo R. 2013. Acidocalcisomes of *Trypanosoma brucei* have an inositol 1,4,5-trisphosphate receptor that is required for growth and infectivity. *Proc Natl Acad Sci U S A.* 110:1887–1892.
- Iino M. 2010. Spatiotemporal dynamics of Ca²⁺ signaling and its physiological roles. *Proc Jpn Acad Ser B Phys Biol Sci.* 86:244–256.
- Joseph SK, Boehning D, Pierson S, Nicchitta CV. 1997. Membrane insertion, glycosylation, and oligomerization of inositol trisphosphate receptors in a cell-free translation system. *J Biol Chem.* 272: 1579–1588.
- Katoh K, Misawa K, Kuma K, Miyata T. 2002. MAFFT: a novel method for rapid multiple sequence alignment based on fast Fourier transform. *Nucleic Acids Res.* 30:3059–3066.
- King N. 2004. The unicellular ancestry of animal development. *Dev Cell.* 7:313–325.
- King N, Westbrook MJ, Young SL, Kuo A, Abedin M, Chapman J, Fairclough S, Hellsten U, Isogai Y, Letunic I, et al. 2008. The genome of the choanoflagellate *Monosiga brevicollis* and the origin of metazoans. *Nature* 451:783–788.
- Krinke O, Novotna Z, Valentova O, Martinec J. 2007. Inositol trisphosphate receptor in higher plants: is it real? *J Exp Bot.* 58: 361–376.
- Ladenburger EM, Sehring IM, Korn I, Plattner H. 2009. Novel types of Ca²⁺ release channels participate in the secretory cycle of *Paramecium* cells. *Mol Cell Biol.* 29:3605–3622.
- Lartillot N, Lepage T, Blanquart S. 2009. PhyloBayes 3: a Bayesian software package for phylogenetic reconstruction and molecular dating. *Bioinformatics* 25:2286–2288.
- Le SQ, Gascuel O. 2008. An improved general amino acid replacement matrix. *Mol Biol Evol.* 25:1307–1320.
- Owczarzak A, Stibbs HH, Bayne CJ. 1980. The destruction of *Schistosoma mansoni* mother sporocysts in vitro by amoebae isolated from *Biomphalaria glabrata*: an ultrastructural study. *J Invertebr Pathol.* 35:26–33.
- Plattner H, Verkhatsky A. 2013. Ca²⁺ signalling early in evolution—all but primitive. *J Cell Sci.* 126:2141–2150.
- Robinson MD, McCarthy DJ, Smyth GK. 2010. edgeR: a Bioconductor package for differential expression analysis of digital gene expression data. *Bioinformatics* 26:139–140.
- Ruiz-Trillo I, Inagaki Y, Davis LA, Sperstad S, Landfald B, Roger AJ. 2004. *Capsaspora owczarzaki* is an independent opisthokont lineage. *Curr Biol.* 14:R946–R947.
- Ruiz-Trillo I, Roger AJ, Burger G, Gray MW, Lang BF. 2008. A phylogenomic investigation into the origin of metazoa. *Mol Biol Evol.* 25: 664–672.
- Sebe-Pedros A, de Mendoza A, Lang BF, Degnan BM, Ruiz-Trillo I. 2011. Unexpected repertoire of metazoan transcription factors in the unicellular holozoan *Capsaspora owczarzaki*. *Mol Biol Evol.* 28: 1241–1254.
- Sebe-Pedros A, Irimia M, Del Campo J, Parra-Acero H, Russ C, Nusbaum C, Blencowe BJ, Ruiz-Trillo I. 2013. Regulated aggregative multicellularity in a close unicellular relative of metazoa. *Elife* 2:e01287.
- Sienaert I, Missiaen L, De Smedt H, Parys JB, Sipma H, Casteels R. 1997. Molecular and functional evidence for multiple Ca²⁺-binding domains in the type 1 inositol 1,4,5-trisphosphate receptor. *J Biol Chem.* 272:25899–25906.
- Stamatakis A. 2006. RAxML-VI-HPC: maximum likelihood-based phylogenetic analyses with thousands of taxa and mixed models. *Bioinformatics* 22:2688–2690.
- Steenkamp ET, Wright J, Baldauf SL. 2006. The protistan origins of animals and fungi. *Mol Biol Evol.* 23:93–106.
- Stibbs HH, Owczarzak A, Bayne CJ, DeWan P. 1979. Schistosome sporocyst-killing Amoebae isolated from *Biomphalaria glabrata*. *J Invertebr Pathol.* 33:159–170.
- Suga H, Chen Z, de Mendoza A, Sebe-Pedros A, Brown MW, Kramer E, Carr M, Kerner P, Vervoort M, Sanchez-Pons N, et al. 2013. The *Capsaspora* genome reveals a complex unicellular prehistory of animals. *Nat Commun.* 4:2325.
- Sugawara H, Kurosaki M, Takata M, Kurosaki T. 1997. Genetic evidence for involvement of type 1, type 2 and type 3 inositol 1,4,5-trisphosphate receptors in signal transduction through the B-cell antigen receptor. *EMBO J.* 16:3078–3088.
- Taylor CW, Genazzani AA, Morris SA. 1999. Expression of inositol trisphosphate receptors. *Cell Calcium* 26:237–251.
- Tisi R, Belotti F, Wera S, Winderickx J, Thevelein JM, Martegani E. 2004. Evidence for inositol triphosphate as a second messenger for glucose-induced calcium signalling in budding yeast. *Curr Genet.* 45: 83–89.
- Torruella G, Derelle R, Paps J, Lang BF, Roger AJ, Shalchian-Tabrizi K, Ruiz-Trillo I. 2012. Phylogenetic relationships within the Opisthokonta based on phylogenomic analyses of conserved single-copy protein domains. *Mol Biol Evol.* 29:531–544.
- Trapnell C, Roberts A, Goff L, Pertea G, Kim D, Kelley DR, Pimentel H, Salzberg SL, Rinn JL, Pachter L. 2012. Differential gene and transcript expression analysis of RNA-seq experiments with TopHat and Cufflinks. *Nat Protoc.* 7:562–578.
- Tu H, Nosyreva E, Miyakawa T, Wang Z, Mizushima A, Iino M, Bezprozvanny I. 2003. Functional and biochemical analysis of the type 1 inositol (1,4,5)-trisphosphate receptor calcium sensor. *Biophys J.* 85:290–299.
- Vanderheyden V, Devogelaere B, Missiaen L, De Smedt H, Bultynck G, Parys JB. 2009. Regulation of inositol 1,4,5-trisphosphate-induced Ca²⁺ release by reversible phosphorylation and dephosphorylation. *Biochim Biophys Acta.* 1793:959–970.
- Varnai P, Balla A, Hunyady L, Balla T. 2005. Targeted expression of the inositol 1,4,5-trisphosphate receptor (IP3R) ligand-binding domain releases Ca²⁺ via endogenous IP3R channels. *Proc Natl Acad Sci U S A.* 102:7859–7864.
- Verkhatsky A, Parpura V. 2014. Calcium signalling and calcium channels: evolution and general principles. *Eur J Pharmacol.* 739:1–3.
- Vermassen E, Parys JB, Mauger JP. 2004. Subcellular distribution of the inositol 1,4,5-trisphosphate receptors: functional relevance and molecular determinants. *Biol Cell.* 96:3–17.
- Yoshikawa F, Morita M, Monkawa T, Michikawa T, Furuichi T, Mikoshiba K. 1996. Mutational analysis of the ligand binding site of the inositol 1,4,5-trisphosphate receptor. *J Biol Chem.* 271: 18277–18284.

- Yule DI, Betzenhauser MJ, Joseph SK. 2010. Linking structure to function: recent lessons from inositol 1,4,5-trisphosphate receptor mutagenesis. *Cell Calcium* 47:469–479.
- Zhang D, Boulware MJ, Pendleton MR, Nogi T, Marchant JS. 2007. The inositol 1,4,5-trisphosphate receptor (Itrp) gene family in *Xenopus*: identification of type 2 and type 3 inositol 1,4,5-trisphosphate receptor subtypes. *Biochem J.* 404:383–391.
- Zucchi R, Ronca-Testoni S. 1997. The sarcoplasmic reticulum Ca²⁺ channel/ryanodine receptor: modulation by endogenous effectors, drugs and disease states. *Pharmacol Rev.* 49:1–51.